

## Investigation of the Effects of Different Land Use and Land Cover Patterns on Mesoscale Meteorological Simulations in the Taiwan Area

FANG-YI CHENG, YU-CHING HSU, AND PAY-LIAM LIN

*Department of Atmospheric Sciences, National Central University, Jhongli City, Taiwan*

TANG-HUANG LIN

*Center for Space and Remote Sensing Research, National Central University, Jhongli City, Taiwan*

(Manuscript received 9 April 2012, in final form 11 September 2012)

### ABSTRACT

The U.S. Geological Survey (USGS) land use (LU) data employed in the Weather Research and Forecasting (WRF) model classify most LU types in Taiwan as mixtures of irrigated cropland and forest, which is not an accurate representation of current conditions. The WRF model released after version 3.1 provides an alternative LU dataset retrieved from 2001 Moderate Resolution Imaging Spectroradiometer (MODIS) satellite products. The MODIS data correctly identify most LU-type distributions, except that they represent western Taiwan as being extremely urbanized. A new LU dataset, obtained using 2007 Système Probatoire d'Observation de la Terre (SPOT) satellite imagery [from the National Central University of Taiwan (NCU)], accurately shows the major metropolitan cities as well as other land types. Three WRF simulations were performed, each with a different LU dataset. Owing to the overestimation of urban area in the MODIS data, WRF-MODIS overpredicts daytime temperatures in western Taiwan. Conversely, WRF-USGS underpredicts daytime temperatures. The temperature variation estimated by WRF-NCU falls between those estimated by the other two simulations. Over the ocean, WRF-MODIS predicts the strongest onshore sea breezes, owing to the enhanced temperature gradient between land and sea, while WRF-USGS predicts the weakest onshore flow. The intensity of the onshore breeze predicted by WRF-NCU is between those predicted by WRF-MODIS and WRF-USGS. Over Taiwan, roughness length is the key parameter influencing wind speed. WRF-USGS significantly overpredicts the surface wind speed owing to the shorter roughness length of its elements, while the surface wind speeds estimated by WRF-NCU and WRF-MODIS are in better agreement with the observed data.

### 1. Introduction

The twin processes of urbanization and deforestation occurring over the past few decades have slowly changed the land surface characteristics of Taiwan; these changes modify the local circulation and boundary layer structures. For example, the urbanization process increases temperature due to changes in land surface characteristics, such as increased paving, rooftops, buildings, and other urban infrastructure. Meanwhile, deforestation will affect evapotranspiration processes.

Over the past few decades, land use (LU) and land cover (LC) characteristics in Taiwan have changed substantially. Major cities such as Taipei, Taichung, and

Kaohsiung have evolved into megacities, accompanied by the removal of croplands and trees on the outskirts and further urbanization in different parts of the metropolitan area. Such changes have modified local weather conditions, including the land–sea-breeze (LSB) circulation pattern and urban heat island effects (Tai et al. 2008).

Taiwan is an island, with the Central Mountain Range (CMR) running from the north of the island to the south. When synoptic-scale forcing is weak, the local circulation is normally dominated by the LSB flow. It has been found that the locally produced high ozone events in Taiwan are typically associated with the LSB circulation (Liu et al. 2002; Cheng et al. 2012). To adequately simulate such locally induced circulations and the atmospheric dynamic and thermodynamic processes, a meteorological model requires an LU–LC dataset that accurately represents present surface characteristics.

*Corresponding author address:* Fang-Yi Cheng, 300 Chun-Da Rd., Jhongli City 320, Tao-Yuan County, Taiwan.  
E-mail: bonniecheng18@gmail.com

LU type is an important land surface parameter describing the exchange of heat and momentum between the land and air. It has been demonstrated that LU–LC data can have a significant effect on meteorological simulations. For example, Cheng and Byun (2008) found that the update of the LU–LC data using Landsat-derived datasets successfully improved the prediction of transport and mixing processes in the planetary boundary layer (PBL). Grossman-Clarke et al. (2005) divided the U.S. Geological Survey (USGS) urban category into three classes (urban built up, urban mesic residential, and urban xeric residential) based on the distribution of vegetation and irrigation. The new LU classification had an apparent impact on turbulent heat fluxes and PBL evolution, and improved the prediction of daytime and nighttime temperatures. Similar studies have also been conducted by Lam et al. (2006), Lo and Quattrochi (2003), and Civerolo et al. (2007).

For applications in the Taiwan area, Tai et al. (2008) performed Weather Research and Forecasting (WRF) model simulations by replacing the original USGS 25-category LU data with a new LU dataset prepared by China Technical Consultants, Inc. (CTCI). The new LU data were retrieved from aerial photographs collected from 1999 to 2001. These CTCI LU–LC data correctly identify the urbanization processes in the cities of Taipei, Taichung, and Kaohsiung; however, most parts of the CMR area were assigned to the mixed-forest-type LU category without additional detailed classification. The simulation result showed that the model was able to produce a reasonable response to the improved LU dataset in terms of ground temperature, latent heat flux, and sensible heat flux. The use of different LU data also contributed to the differences in simulated precipitation, surface temperature, and wind field. One major concern regarding this dataset is that aerial photographs collected from 1999 to 2001 may have failed to capture very recent urban expansion. Another study conducted by Lin et al. (2011) coupled a WRF model with an urban canopy model and reclassified the LU types from 1999 Moderate Resolution Imaging Spectroradiometer (MODIS) satellite images. The simulation results improved predictions of the patterns of accumulated rainfall when compared with the simulation performed using the USGS LU data. In comparison with the LU data prepared by CTCI, the 1999 MODIS LU data better represent mountainous areas as a mixture of deciduous and needleleaf forest types while the western side of the country is extremely urbanized.

The current USGS 25-category LU–LC data available for WRF models have a resolution of roughly 1 km (reference year 1990), with some of the components originating from a dataset compiled in the 1970s. The

problems introduced by the use of the outdated LU–LC data currently available for WRF meteorological modeling have been remedied with support from the Center for Space and Remote Sensing Research at National Central University (NCU). New LU–LC data have been derived using 2007 Système Probatoire d'Observation de la Terre (SPOT) satellite images; we refer to these updated LU datasets as NCU.

The objectives of this study are 1) to demonstrate the effects of using different LU–LC datasets on the simulated meteorological fields, 2) to establish the importance of using accurate LU–LC datasets in the simulated temperature, wind speed, and surface heat flux components and in LSB dynamics, and 3) to improve weather prediction capability in Taiwan through the update of the LU–LC datasets.

The episode characterization and model configuration are described in section 2. The classification of the NCU LU data and comparison with other LU datasets are described in section 3. The meteorological simulation results are reviewed in section 4, and some conclusions are summarized in section 5.

## 2. Episode characterization and model configuration

In this study, WRF, version 3.2.1, was selected for the meteorological simulation. The WRF model is a meso-scale numerical weather prediction system designed to serve both operational forecasting and atmospheric research needs (Michalakes et al. 2001; Klemp et al. 2007) and it has been widely used in the meteorological modeling community. The simulation episode runs from 7 to 11 May 2007. On 7 May, a continental anticyclone originating from mainland China moved to the South China Sea and Taiwan was under the influence of north-easterly to easterly flow. On 8 May, a cold pressure system moved eastward and the wind direction in Taiwan changed to southeasterly. On 9 May, the cold high pressure system left Taiwan and, with the weak influence of the synoptic forcing, the local circulation was dominated by LSB flow in western Taiwan. Figure 1a shows the surface weather map generated by the Japan Meteorology Agency at 0800 local standard time (LST) 9 May 2007. On 10 and 11 May, Taiwan was under the weak influence of a cold pressure system that was situated at the northern end of the country. Northern Taiwan was affected by easterly wind, while other areas in Taiwan were affected by weakly southeasterly flow.

The simulation domain is shown in Fig. 1b. The coarse domain was set to have a resolution of 81 km, ranging down to resolutions of 27, 9, and 3 km. The finest domain covers Taiwan and the surrounding ocean. The

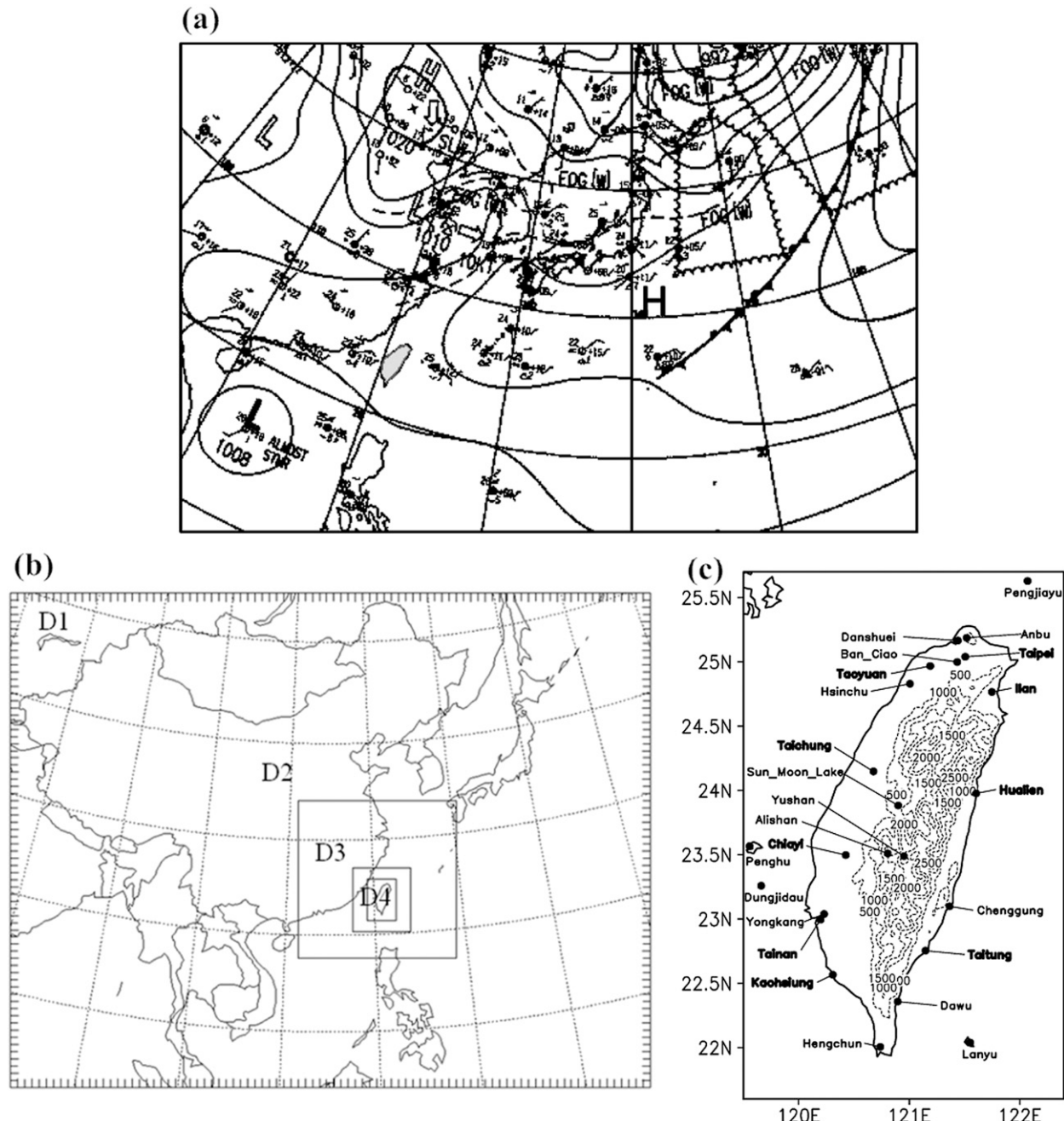


FIG. 1. (a) Surface weather map at 0800 LST 9 May 2007, (b) model simulation domain, and (c) observation monitoring stations (black dots) with dashed contour lines representing the terrain height (m).

vertical layer was composed of 35 full sigma levels, 16 of them within the lowest 1.5 km, with the lowest layer at around 16 m. The model top was at 100 hPa. The initial and boundary conditions were acquired from the National Centers for Environmental Prediction's (NCEP) Final Analysis (FNL) of global data. The analysis nudging approach was applied above the boundary layer for wind, temperature, and water vapor through domains 1–3

to allow for larger-scale forcing to be used to nudge the model simulation toward the reanalysis field.

The WRF physical options include the following: Kain–Fritsch cumulus schemes (Kain and Fritsch 1993) (not used at the 9- and 3-km domains), a Dudhia shortwave radiation scheme (Dudhia 1989), the Rapid Radiative Transfer Model longwave radiation scheme (Mlawer et al. 1997), a Yonsei University PBL scheme (Hong et al.

TABLE 1. Land use mapping from NCU to USGS classifications.

NCU	USGS
Water body	Water body
Building	Urban
Sea	Water body
Road	Urban
Riverbed	Water
Fallow land	Dry-irrigated cropland or dry cropland
Grassland	Grassland
Cropland	Dry-irrigated cropland or irrigated land
Forest	Mixed forest
No data	Closest type
Unidentified	Closest type

2006), and the Noah land surface model (LSM) (Chen and Dudhia 2001). The Noah LSM incorporates the evapotranspiration process, and soil moisture is updated with recent precipitation and evapotranspiration through the initialization data. To fully exploit the new land surface data, an LSM incorporating sufficient physical processes (such as the Noah LSM) is required for meteorological simulation.

Figure 1c illustrates the locations of the Central Weather Bureau (CWB) stations in Taiwan that are used to evaluate model performance. Regions of sloping terrain can be identified based on the topographic height distribution, as shown by the contour line in Fig. 1c. The observed data include temperature and wind speed and direction. In particular, data from the flux tower located at Chiayi are used to evaluate surface flux components. The locations of major metropolitan cities (Taipei, Taoyuan, Taichung, Chiayi, Tainan, Kaohsiung, Ilan, Hualien, and Taitung) are also identified.

### 3. Land use and land cover data

The NCU LU data were retrieved from SPOT satellite images with resolution of 10 m that were collected on 14 October 2007. There are 11 LU classifications, which had to be remapped to the corresponding USGS type. Table 1 is the corresponding mapping table. Most of the classifications from the NCU data could be assigned directly, as they corresponded to the USGS types; however, classification for croplands and fallow land was not straightforward. Cropland could be remapped either as dry-irrigated cropland or irrigated land depending on the style of cultivation. Taiwan's main crops are rice, sugar cane, fruits, and vegetables. Rice paddy areas were assigned to the irrigated cropland LU; all other crops were classified as dry-irrigated cropland. Information on crop varieties was obtained from the land use program under the Ministry of the Interior. Areas where

fallow land was recognized were reclassified. In this study, the episode studied was from 7 to 11 May 2007, that is, during a period where the land was being cultivated. Consequently, the areas classified as fallow land were assigned to the mixed dry-irrigated cropland category if the land was under cultivation; otherwise, they were identified as dry cropland.

Figure 2a shows the LU types at 3-km resolution; from left to right, they are the USGS, MODIS, and NCU classifications. In the USGS data, almost all of the western side of the country was classified as irrigated cropland, a completely outdated classification that does not take into account urbanization processes over recent decades. Additionally, the coverage of forestlands has been erroneously located. The MODIS LU classifications were retrieved from the 2001 MODIS satellite products and were provided from the WRF model released after version 3.1. Relative to the USGS data, the 2001 MODIS LU data more accurately identified the distribution of forestlands; however, urbanization (indicated by the red color in the figure) was overestimated on the western side of the country. In the NCU LU data, the major metropolitan cities were identified accurately, as were irrigated croplands and forested areas. Figure 2b is similar to Fig. 2a, but has been enlarged to encompass the area of northern Taiwan.

Table 2 lists the percentages of each LU distribution class by area over the land surface of Taiwan. The major differences in LU distribution among the three LU datasets are reflected in the urban, cropland, and forestland categories. For the USGS data, the coverage of urban areas was very small (<0.2%); 56% of the area was classified as irrigated cropland and 25% as forestlands. Conversely, for the 2001 MODIS data, 17% was classified as urban area, 14% as cropland, and 66% as forestlands. Based on the NCU dataset, 5% was classified as urban, 22% as cropland, and 65% as forestlands.

One disadvantage of the NCU data is that the majority of the LU types over the mountainous regions are classified as mixed forest types without consideration of detailed characteristics, such as whether they are deciduous or needleleaf forests. This limitation is due to the spectral resolution of the onboard satellite sensors, such as the SPOT High Resolution Stereo or the Landsat Thematic Mapper, which is too coarse to provide sufficient radiometric features for discrimination. Furthermore, the slope and aspect of the terrain and non-Lambertian surface reflectance create geometric variations from the forest reflectivity, particularly over mountainous areas.

Three WRF sensitivity studies were designed to investigate the impact of different LU datasets (the original USGS, MODIS, and new NCU datasets) on meteorological simulations; we refer to these as WRF-USGS,

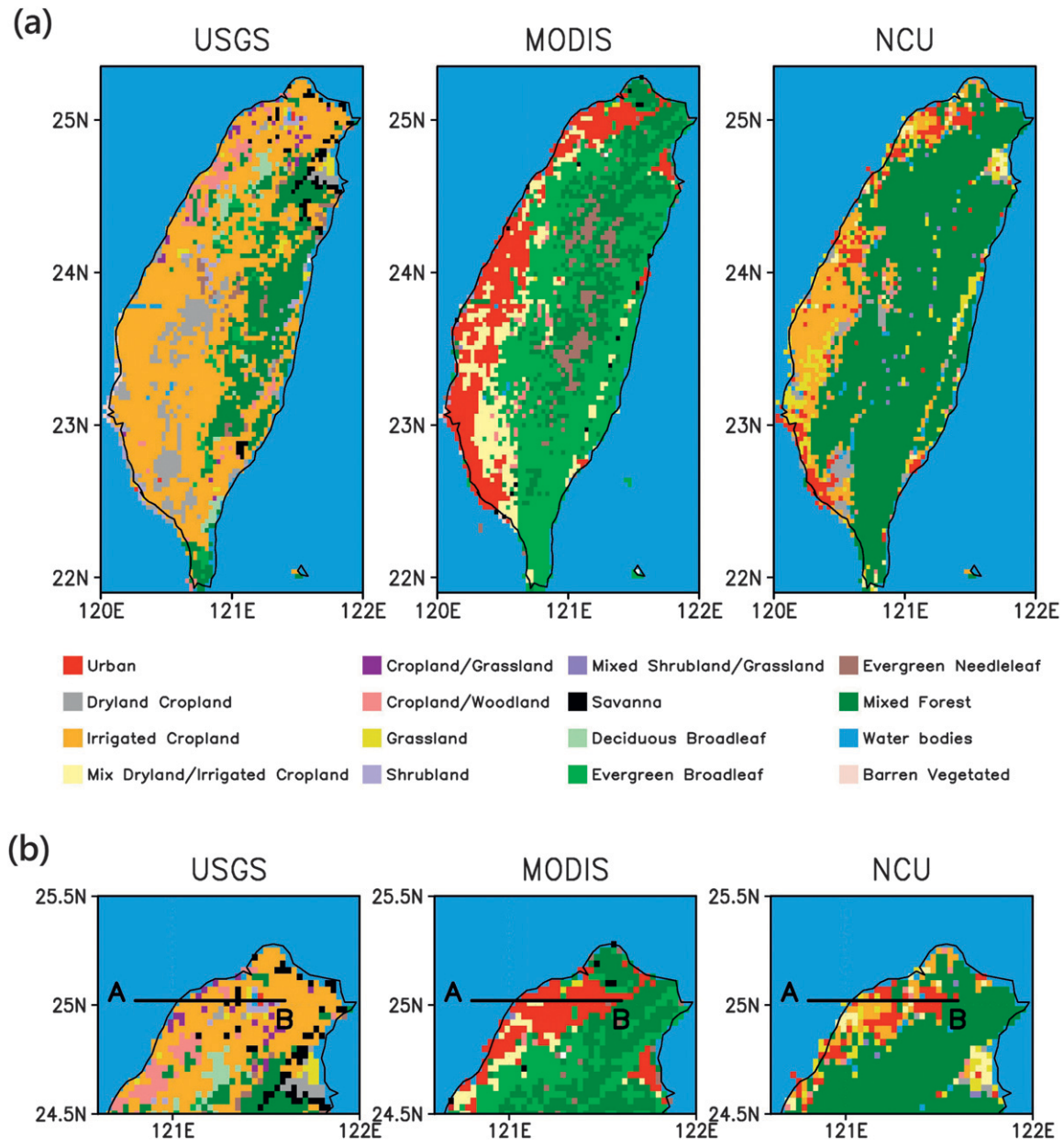


FIG. 2. (a) The LU distribution from (left) USGS, (center) MODIS, and (right) NCU data at 3-km resolution. (b) Enlargement encompassing the area of northern Taiwan.

WRF-MODIS, and WRF-NCU, respectively. The NCU LU data correctly represented the major metropolitan cities as urban LU type. Conversely, the USGS data represented these highly populated regions as underdeveloped rural areas. This difference between the WRF-USGS and WRF-NCU results can be used to study the impact of enhanced anthropogenic activity due to urbanization processes on local-scale meteorological simulation. We focused mainly on a comparison between the WRF-USGS and WRF-NCU simulations, while the results from the WRF-MODIS served as additional information

to understand the effects of extreme urbanization processes on meteorological simulations.

#### 4. Simulation results

##### a. Spatial comparison of the simulations (temperature, wind fields, roughness length, and Bowen ratio)

Figure 3 illustrates the 2-m temperature distributions. The top panel in Fig. 3 shows the temperature fields

TABLE 2. Percentages of each LU distribution class by area over the land surface of Taiwan (blank for zero distribution).

	USGS	MODIS	NCU
Urban	0.158	16.895	5.113
Dry cropland	8.171		3.057
Irrigated cropland	56.458		15.156
Mixed dry-irrigated		13.073	1.502
Cropland–grassland	1.292		0.395
Cropland–woodland	2.794	1.45	1.529
Grassland	1.133	0.659	5.166
Shrub land	1.871	0.264	0.026
Mixed Shrub–grassland		0.132	0.712
Savanna	2.003	0.158	
Deciduous broadleaf	1.898		
Deciduous needleleaf			
Evergreen broadleaf	2.609	42.462	
Evergreen needleleaf	2.478	4.823	0.554
Mixed forest	18.608	18.872	64.839
Water bodies		0.712	1.95
Herbaceous wetland			0.026
Barren vegetated	0.501	0.264	
Wooded tundra	0.026		

averaged from 1000 to 1600 LST 9 May as representative of the daytime average. The bottom panel in Fig. 3 shows the data averaged from 2200 LST 9 May to 0400 LST 10 May as representative of the nighttime average. During the day, the major temperature difference between WRF-USGS and WRF-NCU appeared in urban areas, particularly in the cities of Taipei, Taichung, and Kaohsiung. WRF-MODIS predicted the highest temperatures in western Taiwan due to the overly urbanized surface structures distributed in that area. Through the night, the temperature was also raised in these cities in the WRF-NCU simulation compared to the WRF-USGS run, while WRF-MODIS still predicted the highest temperatures in western Taiwan. Near the mountainous regions, even though the LU distribution was distinct among the three datasets, the simulated temperature fields behaved similarly in all model results. In fact, the temperature distribution over the CMR region was affected more by topographical height than by LU–LC changes. The comparison indicated that, even though the NCU LU data could not distinguish detail in the mountainous regions, this did not have a significant impact on temperature comparisons in the CMR region, as it was the terrain height that played the major role in the determination of the temperature distribution.

Figure 4 shows a comparison of wind fields averaged from 1000 to 1600 LST 9 May (top panels) and from 2200 LST 9 May to 0400 LST 10 May 2007. The leftmost plot is from the WRF-NCU run. The center plot in Fig. 4 shows the difference of wind fields, with WRF-USGS subtracted from WRF-NCU, and the rightmost plot the difference with WRF-MODIS subtracted from

WRF-NCU. During the day, the local circulation pattern was dominated by the onshore sea-breeze flow. WRF-NCU predicted stronger onshore flow than WRF-USGS in the offshore areas of western Taiwan, particularly near the coastline of Taoyuan (just south of Taipei) and the Tainan region, which was caused by the enhanced land–sea temperature gradient from the WRF-NCU simulation. Among the three simulations, WRF-MODIS predicted the strongest onshore flow in coastal regions of western Taiwan. Over Taiwan, WRF-NCU predicted lower wind speeds than WRF-USGS, owing to the specification of longer roughness length ( $Z_0$ ) elements (urban structures and forestlands). Through the night, the land-breeze flow was formed over the land and offshore areas of western Taiwan. WRF-NCU predicted weaker offshore flow than WRF-USGS over the areas of megacities such as Taipei and Taichung due to the reduced temperature gradient between the land and the sea. WRF-MODIS predicted the weakest offshore flow of all the runs, especially near the coastal areas on the northwest side of Taiwan. The differences in urban regions were higher during the nighttime than the daytime.

Figure 5 shows the distribution of  $Z_0$  utilized for each individual WRF simulation. In the WRF model, the specified value of  $Z_0$  was obtained from a lookup land use table (Chen and Dudhia 2001) (i.e., by knowing the underlying LU type, land surface parameters such as  $Z_0$  were set accordingly); as a result, the  $Z_0$  distribution was in accordance with the patterns of LU type. Clearly, the lowest value of  $Z_0$  was used in the WRF-USGS run. In the NCU LU data, most of the LU types were replaced with urban and forestlands, which possess higher  $Z_0$  values than the classifications of the USGS LU data. The higher  $Z_0$  would slow the wind flow, as indicated in the center plot of Fig. 4. The major difference in  $Z_0$  between the simulations using MODIS and NCU LU data was in western Taiwan, where a higher  $Z_0$  value was used in the WRF-MODIS run. WRF-NCU predicted higher wind speed than WRF-MODIS in the area where urban type was identified in MODIS LU data but not in NCU LU data (rightmost plot in Fig. 4).

Figure 6 shows the distribution of the Bowen ratio, which is defined as the ratio of the sensible heat flux (SHF) to the latent heat flux (LHF), at 1200 LST 9 May 2007. As expected, the Bowen ratio was smaller over vegetated surfaces where most of the energy goes into transpiration and evaporation, and larger over dry surfaces where most of the energy goes into SHF (Stull 1988). At 1200 LST, the Bowen ratios were consistently higher ( $>5$ ) in the urban areas where higher SHF and lower LHF were simulated. The distribution of the Bowen ratio exhibited a strong correspondence to patterns of LU type. WRF-MODIS predicted the highest Bowen

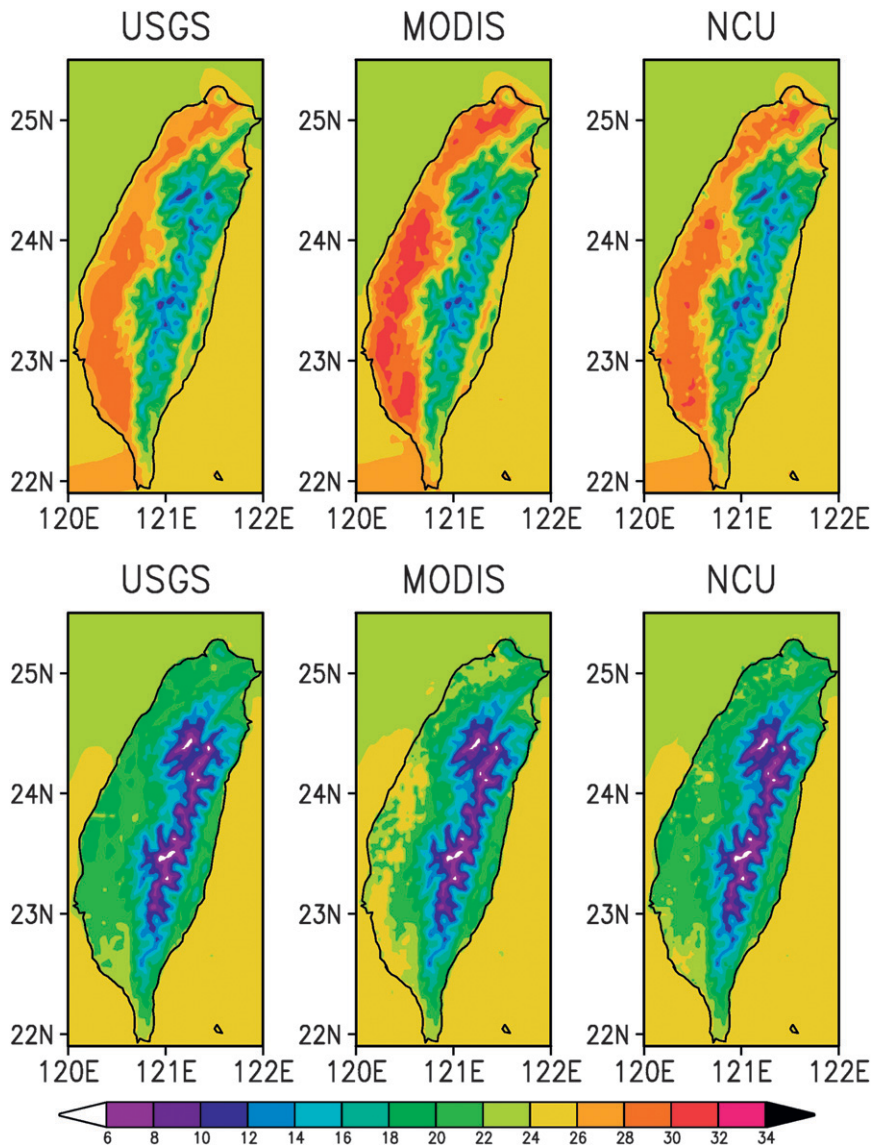


FIG. 3. Comparison of 2-m temperature ( $^{\circ}$ C) averaged (top) from 1000 to 1600 LST 9 May and (bottom) from 2200 LST 9 May to 0400 LST 10 May obtained from simulations using (left) USGS, (center) MODIS, and (right) NCU LU data.

ratio in western Taiwan, while the distributions predicted by WRF-USGS and WRF-NCU were similar, except in areas where an urban LU type was classified from NCU LU data. The Bowen ratio from WRF-USGS was less than one in western Taiwan, indicating that most of the energy was used for evapotranspiration from the croplands. The distribution of the Bowen ratio behaved similarly in the CMR region for all three simulations. This indicates that the change of the LU types over the mountainous regions does not have a significant effect on the surface sensible and latent heat fluxes predictions.

As mentioned before, the terrain height affects the temperature fields more than the LU-LC changes; in addition, the land surface parameters supplied from the lookup land use table does not differ much for different forest types.

#### *b. Vertical cross-sectional analysis*

Figure 7a shows a vertical cross-sectional plot across the Taipei metropolitan area (refer to Fig. 2b for the location) at 1200 LST 9 May 2007 from the WRF-NCU simulation. Across this line, the dominant LU type in the USGS data was irrigated cropland, while the NCU

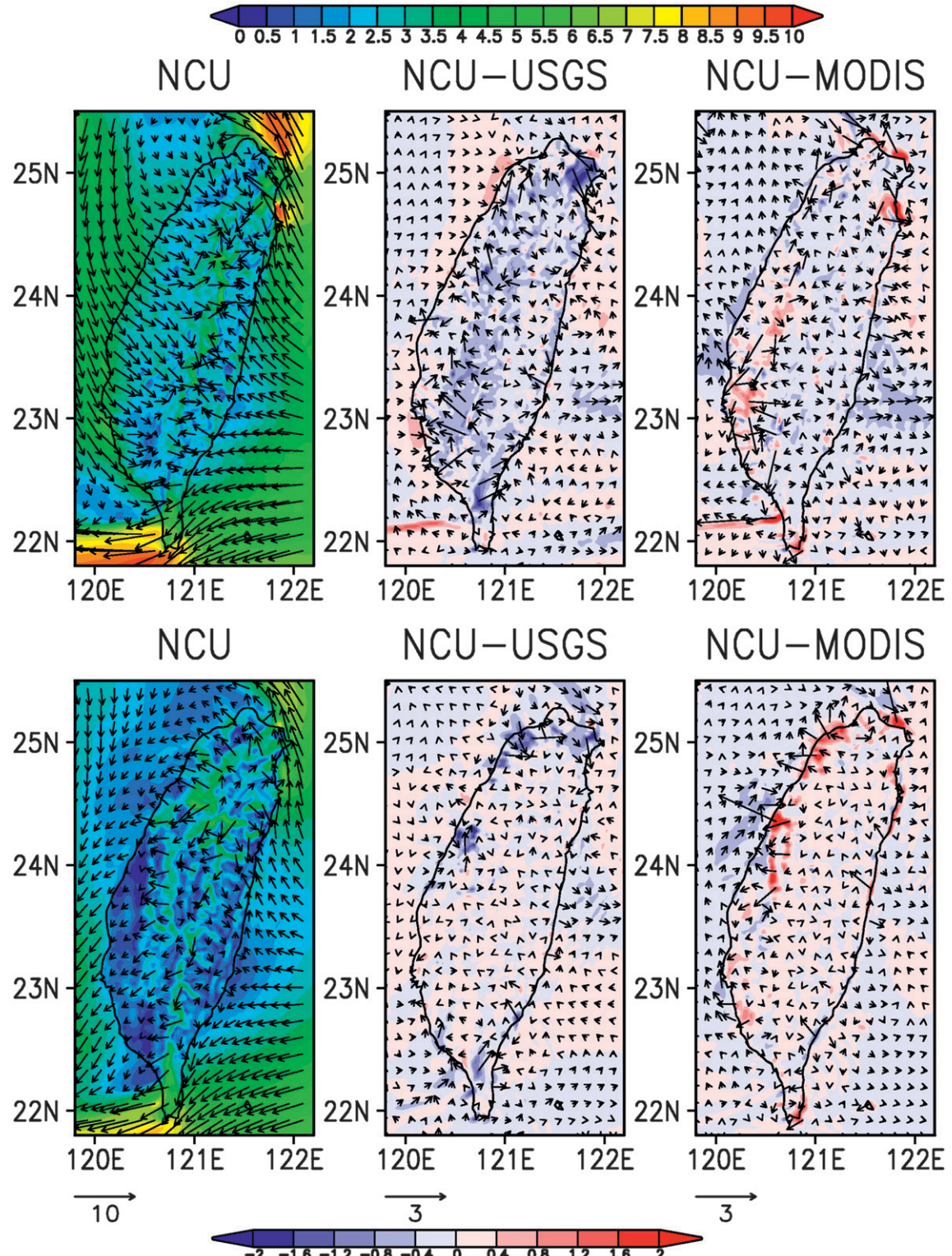


FIG. 4. Comparison of surface wind fields ( $\text{m s}^{-1}$ ) averaged (top) from 1000 to 1600 LST 9 May and (bottom) from 2200 LST 9 May to 0400 LST 10 May. (left) WRF-NCU with color bar shown at the top. Difference with (center) WRF-USGS subtracted from WRF-NCU and (right) with WRF-MODIS subtracted. For the difference plots, the color bar is shown at the bottom.

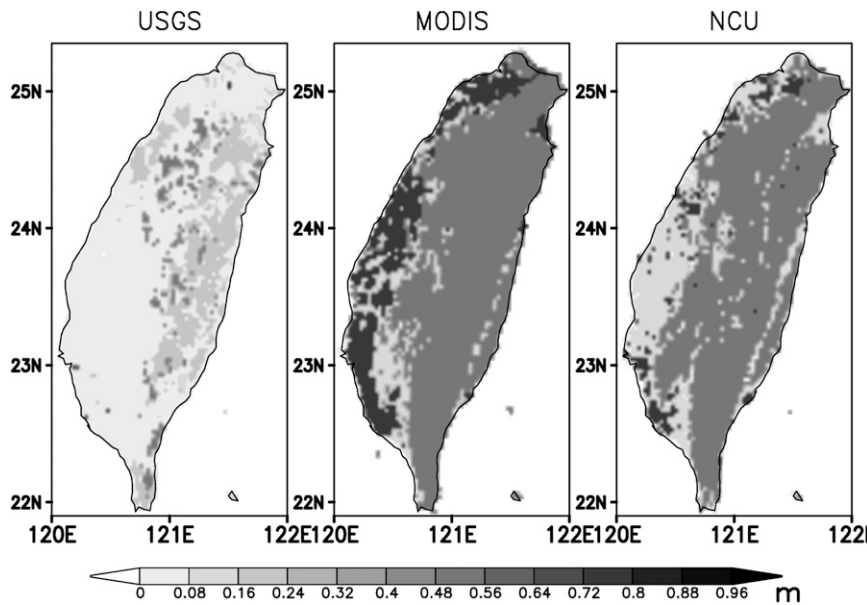


FIG. 5. Distribution of roughness length utilized for (left) WRF-USGS, (center) WRF-MODIS, and (right) WRF-NCU simulations.

data classified it as a mixture of urban, cropland, and forests, and the MODIS data as completely urbanized area. At that time, onshore and upslope flow was simulated in the WRF-NCU simulation. Over the ocean, the onshore sea-breeze flow exhibited a smooth and consistent pattern with very weak vertical motion. Over the landside, due to the effects of surface heating processes, a strong upward motion was simulated at the

hilltop and over Taipei City (near 121.5°E) with a compensating downward movement simulated adjacently. Figure 7b shows the difference in the wind vectors and vertical wind speed simulated by WRF-USGS and WRF-NCU (positive means higher from WRF-NCU). WRF-NCU showed a stronger onshore sea-breeze flow in offshore areas than did the WRF-USGS run. Over the land areas, WRF-NCU predicted

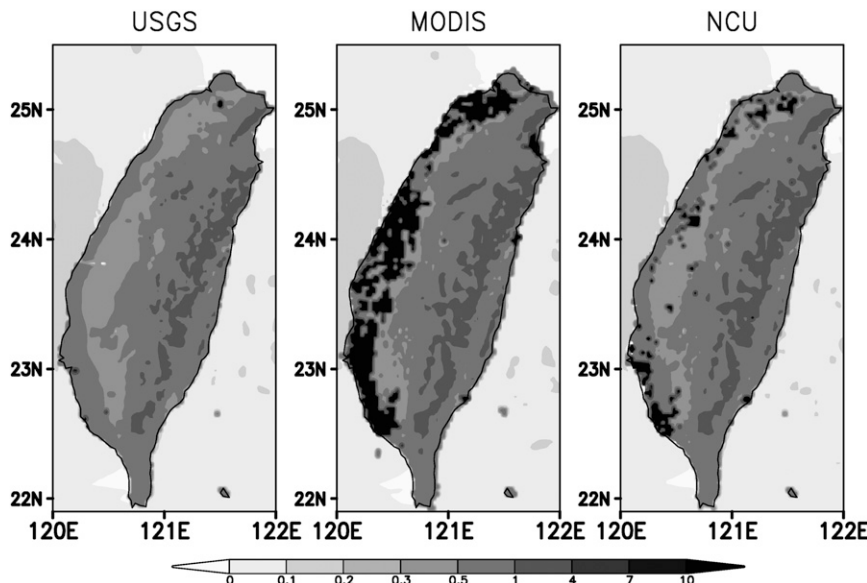


FIG. 6. As in Fig. 5, but for Bowen ratio distribution at 1200 LST 9 May 2007.

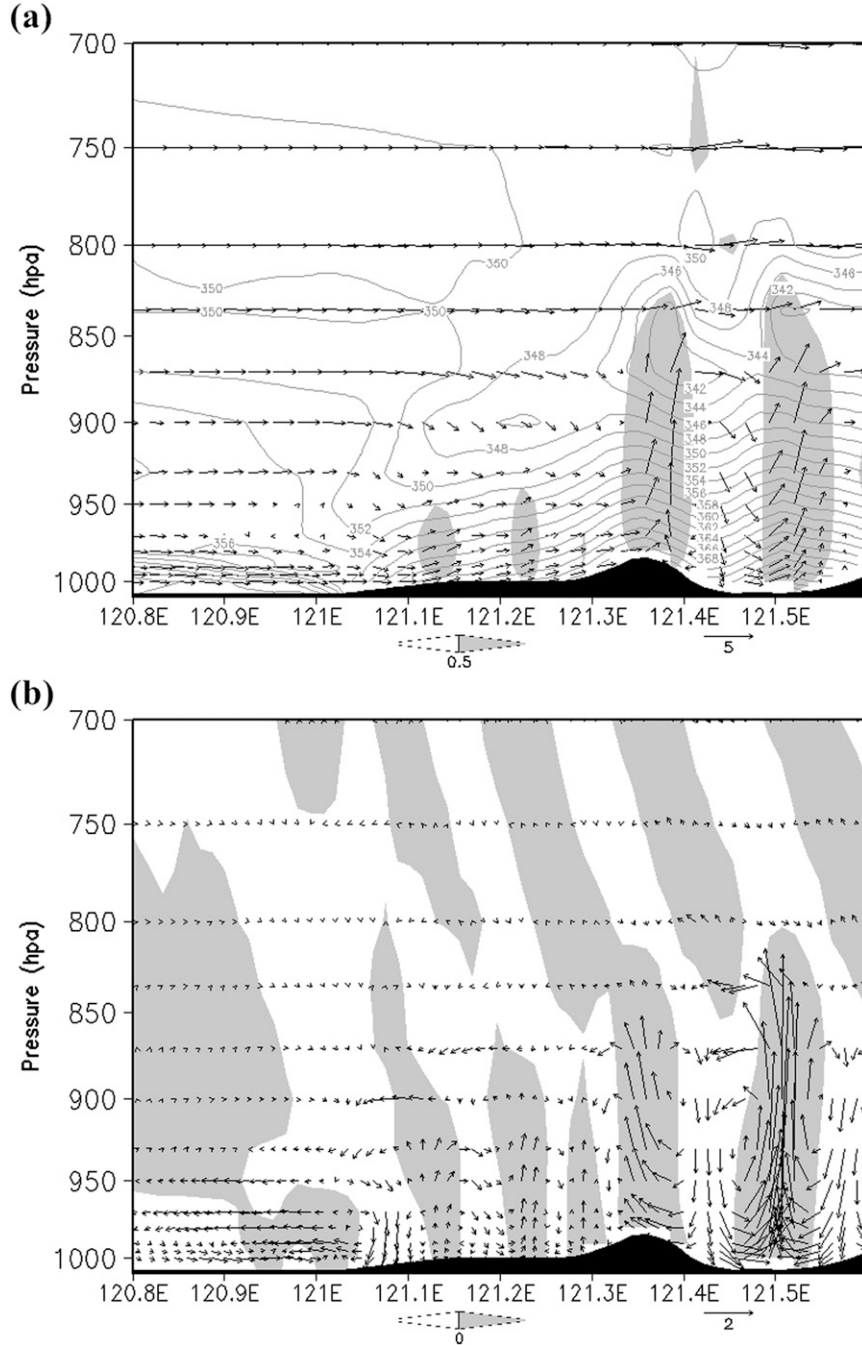


FIG. 7. (a) Vertical cross-sectional analysis at 1200 LST 9 May 2007 from the WRF-NCU simulation. Shading is for vertical wind speed  $> 0.5 \text{ cm s}^{-1}$ . Contour lines are for equivalent potential temperature (K). Wind arrows represent wind vectors having components  $\bar{u}$  and  $\bar{w}$  ( $\text{m s}^{-1}$ ;  $\bar{u}$  is wind along the cross-section line;  $\bar{w}$  is vertical velocity  $\times 10$ ). (b) Difference plot with WRF-USGS subtracted from WRF-NCU. The shading is for differences in vertical wind speed  $> 0 \text{ cm s}^{-1}$ .

stronger convergent flow and upward motion than WRF-USGS, particularly near  $121.5^\circ\text{E}$ , where the major metropolitan area of Taipei is located. The analysis indicated that, with the updated LU-LC data, the underlying

surface was replaced with impervious structures such as roads, parking lots, and buildings, which increased surface heating processes and induced stronger upward motions in Taipei.

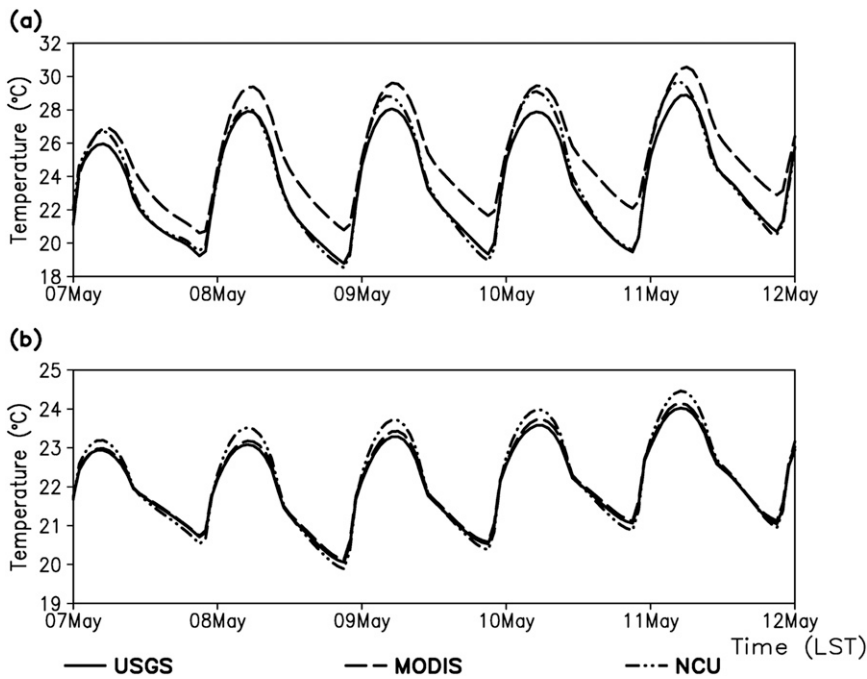


FIG. 8. Time series comparison of the temperature from WRF simulations averaged over space for (a) urban and (b) nonurban areas.

c. *Time series comparison (temperature, wind fields, surface heat fluxes, and soil moisture)*

Figures 8a and 8b show a time series comparison of 2-m temperature from the WRF simulations averaged for urban and nonurban areas, respectively. The urban areas refer to grid points where an urban LU type was specified, while nonurban areas are otherwise indicated. As shown in Fig. 2 and Table 2, the distributions of urban areas were distinct for the three simulations. The difference was more apparent for urban areas than nonurban areas. WRF-MODIS predicted the highest temperatures in urban areas, while WRF-USGS predicted the lowest. The temperature distribution from WRF-NCU was between the other two simulations. For nonurban areas, WRF-NCU predicted higher temperatures during the day and slightly lower temperatures during the night compared to the other simulations.

Figure 9 illustrates the surface wind speed comparison. In the urban areas, WRF-USGS predicted the strongest wind speed, with differences between this simulation and the others reaching  $2 \text{ m s}^{-1}$ ; WRF-NCU predicted the lowest wind speeds. For nonurban areas, the difference between the three simulations was small, with WRF-NCU predicting slightly lower wind speeds than the other simulations.

Figure 10 shows a comparison with the observed surface data at Taipei station. This station was classified as urban type in both the MODIS and NCU LU data,

which represented actual conditions correctly; however, the USGS data treated this site as a type of shrubland. WRF-MODIS predicted the highest 2-m temperatures, while predictions from the other two were similar. For wind speed comparison, there was significant over-prediction by WRF-USGS but the other two runs were in better agreement with the observed data. For the comparison of wind direction, the flow was mostly dominated by northeast-to-easterly flow, except for a time when LSB flow was observed on 9 May. All three runs captured the variations of flow patterns and the turning of the LSB circulation quite well.

Figure 11 shows a comparison of the simulated surface energy fluxes at Taipei station on 9 May. All the simulations predicted higher SHF than LHF. The components of the surface energy fluxes from the shrubland type behaved similarly to those of the urban type. The similarity can be attributed to the use of a high canopy resistance  $R_c$ , which is an important factor in determining the rate of evaporation and transpiration from inside the vegetation canopy to the air; this parameter was calculated according to the formulations of Noilhan and Planton (1989) with the corresponding parameters given from the lookup land use table. The value of  $R_c$  was calculated as follows (Chen and Dudhia 2001):

$$R_c = \frac{R_{c\min}}{\text{LAI} \times F_1 F_2 F_3 F_4}, \quad (1)$$

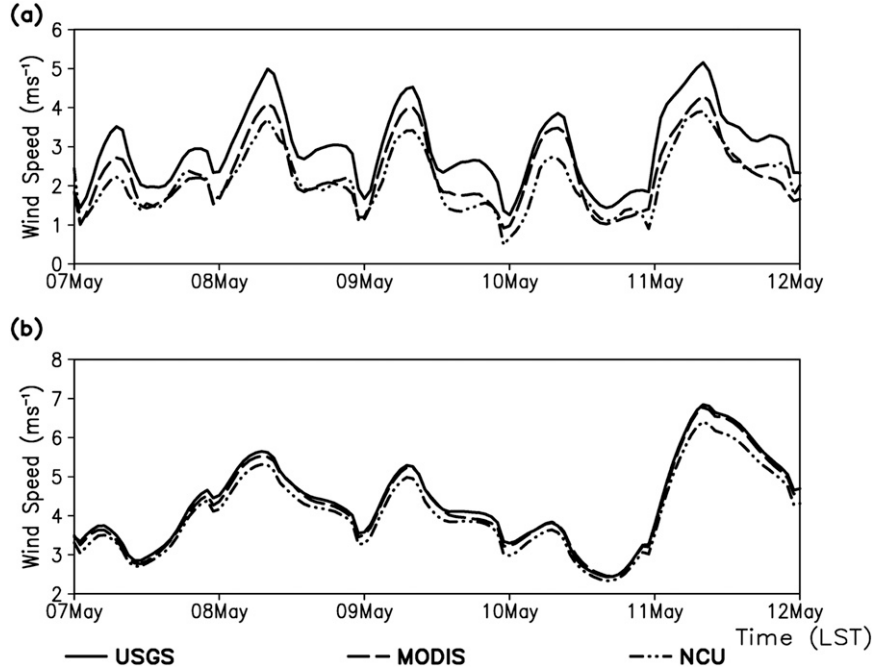
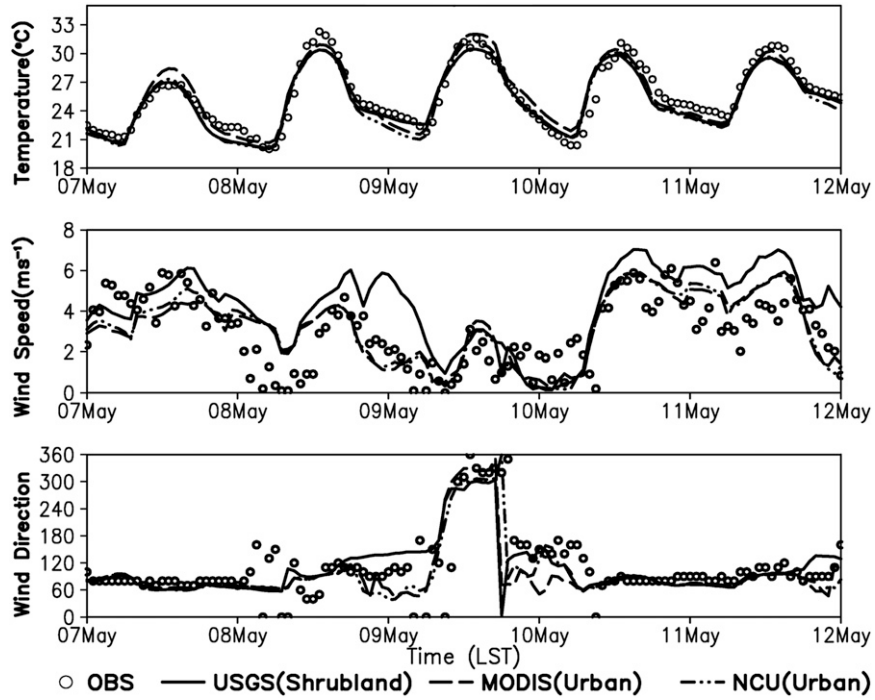


FIG. 9. As in Fig. 8, but for wind speed.

where LAI is the leaf area index,  $F_1$  represents the effects of solar radiation,  $F_2$  takes into account the effect of water stress on surface resistance,  $F_3$  represents the effects of the vapor pressure deficit of the atmosphere,

and  $F_4$  represents the air temperature dependence on surface resistance. The  $R_{c\min}$  is the minimum stomatal resistance. In fact, the default  $R_{c\min}$  defined for shrubland from the lookup table is large (currently  $300 \text{ s m}^{-1}$ ),

FIG. 10. Time series comparison of (top) 2-m temperature, (middle) wind speed, and (bottom) wind direction ( $^{\circ}$ ) at Taipei station.

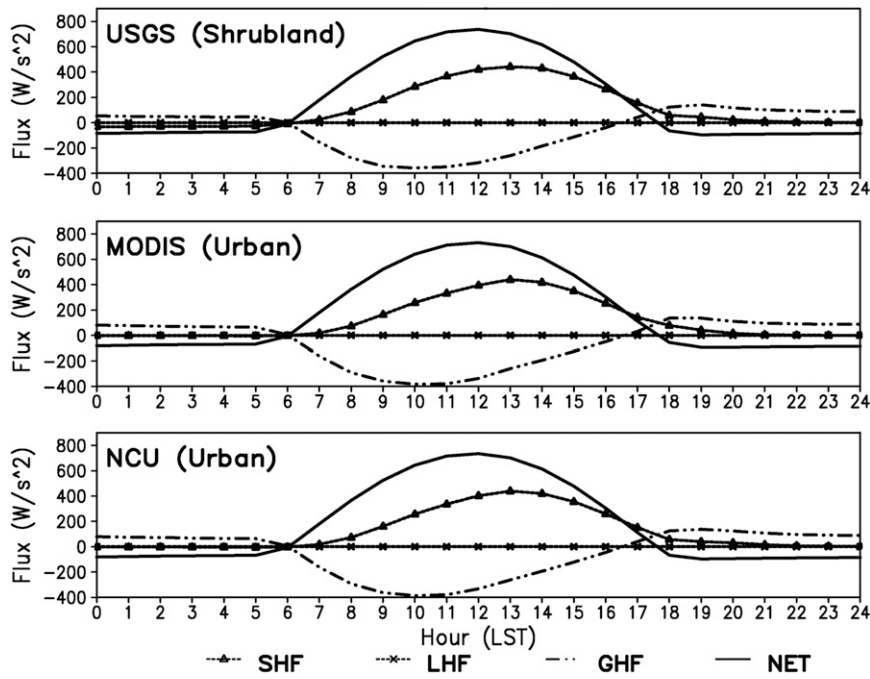


FIG. 11. Comparison of simulated SHF, LHF, GHF, and net radiation (NET) at the Taipei site from (top) WRF-USGS, (middle) WRF-MODIS, and (bottom) WRF-NCU simulations.

which would inhibit evapotranspiration processes. As a result, higher SHF and lower LHF were simulated by WRF-USGS at the Taipei site. The verification of the surface heat flux at this urban site was not possible due to the lack of the observed datasets.

Figures 12 and 13 are similar to Figs. 10 and 11 but for the Chiayi site, which is located in a rural area. The site was classified as an urban type from the MODIS data and as irrigated land from the NCU and USGS datasets. WRF-MODIS showed the highest temperatures and a consistent overestimation, while the other two runs agreed better with the observed data. The wind speed comparison was similar for all three runs with WRF-MODIS showing the lowest wind speed most of the time. For wind direction, unlike the Taipei site, there was a clear turning of the LSB circulation throughout the whole episode at the Chiayi site. This also indicated the distinct atmospheric conditions in northern and southern Taiwan during this episode. As shown in Fig. 13, WRF-MODIS predicted higher SHF than LHF, with very small LHF simulated, while the other two runs behaved similarly with higher LHF than SHF predicted. WRF-MODIS produced the highest estimated values of downward ground heat flux (GHF) among the three simulations.

Fortunately, a flux measurement site located near the Chiayi station was available for comparison. The site

is surrounded by rice paddies and was classified as an urban type from the MODIS data and as irrigated lands from both the USGS and NCU data. Figure 14 compares the simulated SHF and LHF with the observed components. All three runs consistently overpredicted the daytime SHF, with the highest bias from WRF-MODIS. The overprediction from WRF-MODIS contributed to the high temperature bias at the Chiayi site.

The consistent overprediction of SHF can be attributed to the reason that the soil moisture content is too low. Figure 15 shows a comparison of the simulated soil moisture in different soil layers obtained from the three WRF simulations. In the WRF modeling, the soil moisture was initially provided from the reanalysis fields (NCEP FNL data) and updated with recent precipitation and runoff processes. In the rice paddy areas, the underlying soil fields are damp due to high water quantities supplied for irrigation; however, this localized feature is not reflected in the NCEP FNL data due to the coarse spatial resolution ( $1^\circ$ ). As a result, all three runs showed similar distributions of soil moisture throughout the whole period, regardless of the differences in LU type (urban versus irrigated cropland) specified for different WRF simulations. Due to the lack of the observed datasets, the evaluation and comparison of the soil moisture content is not possible. However, Tsai et al. (2007) found that the maximum soil moisture could

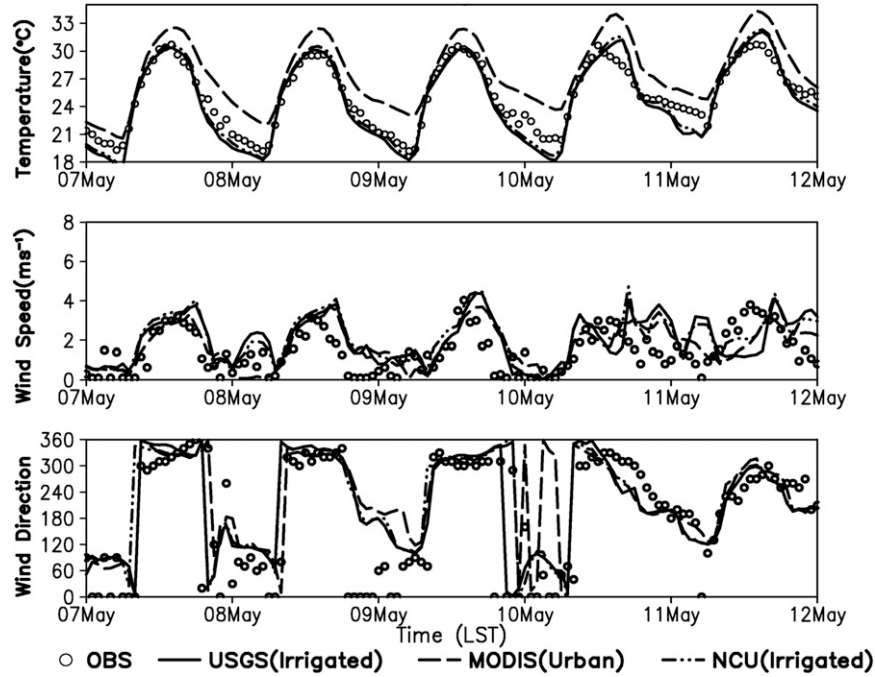


FIG. 12. As in Fig. 10, but for Chiayi station.

reach 0.68 in a rice paddy site in central Taiwan. The simulated soil moisture at the Chiayi site was <0.45 throughout the study period and significantly lower than the observed data based on Tsai et al. (2007). The issues of soil moisture availability are currently under

investigation, so we offer no further discussion on this matter at this time.

For LHF, both WRF-USGS and WRF-NCU agreed well with the measured flux; however, WRF-MODIS showed generally quite low LHF.

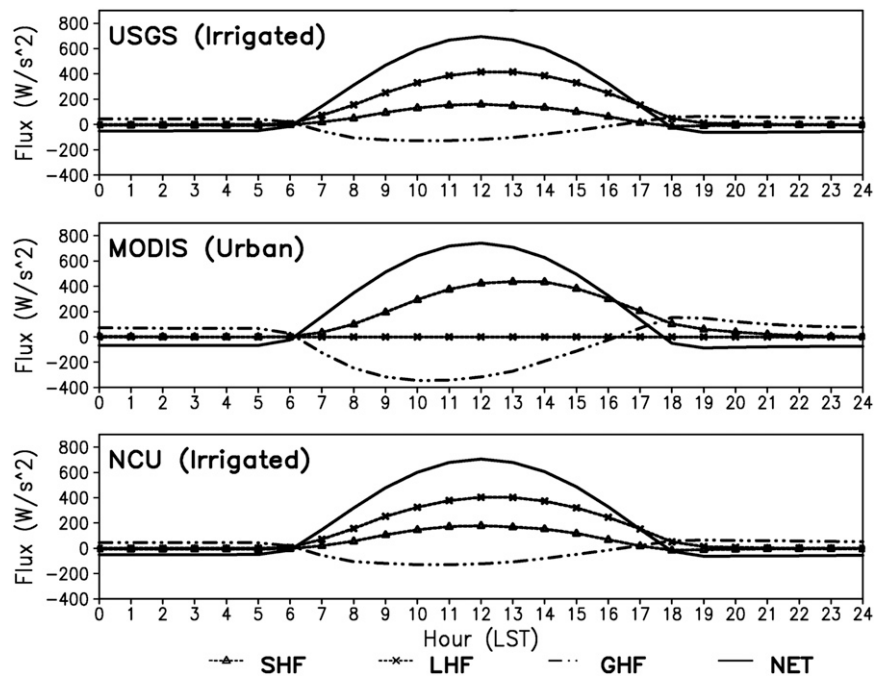


FIG. 13. As in Fig. 11, but for Chiayi station.

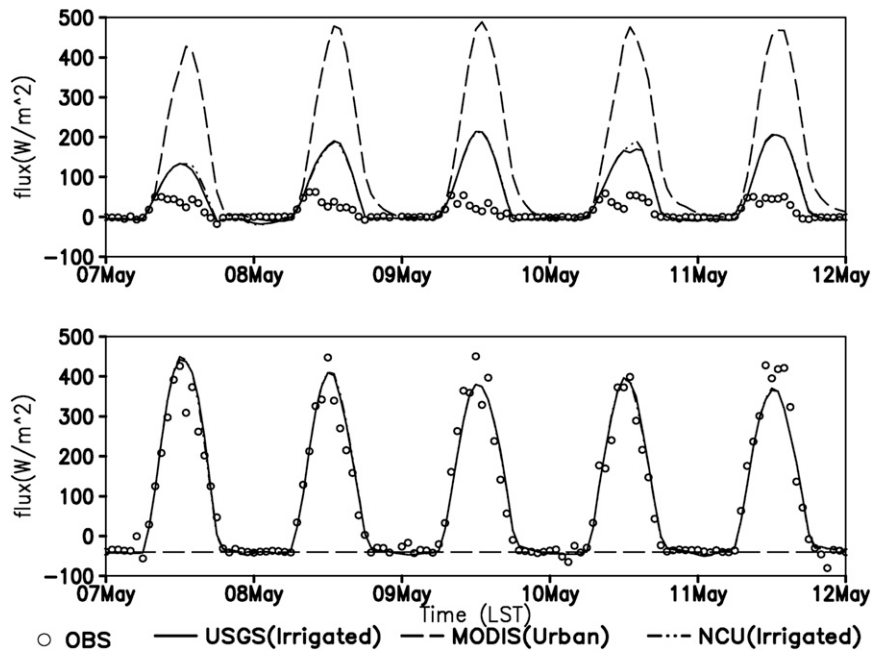


FIG. 14. Comparison of the (top) SHF and (bottom) LHF near the Chiayi station.

The analysis of the surface heat flux components revealed distinct characteristics of surface energy partition processes at the Taipei and Chiayi sites. The land surface was mostly paved with concrete and asphalt in Taipei but

covered by irrigated cropland at the Chiayi site. The misrepresentation of LU type could have erroneously predicted the surface heat flux components, which in turn could have caused the temperature biases near the surface layer.

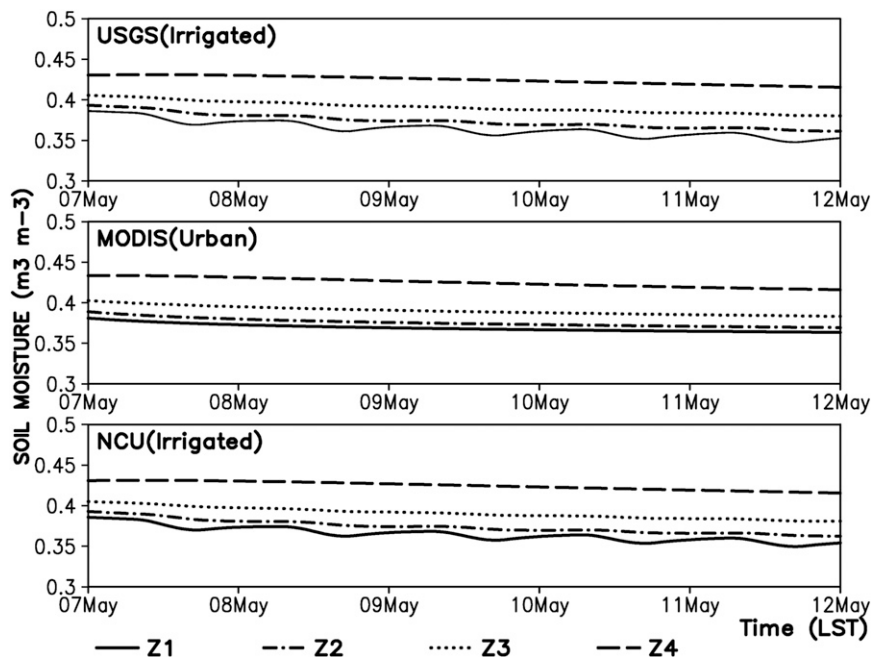


FIG. 15. Comparison of the simulated soil moisture at the Chiayi station from WRF simulations using (top) USGS, (middle) MODIS, and (bottom) NCU LU data from different soil layers. Here, Z1, Z2, Z3, and Z4 represent the thicknesses from the surface of each soil layer and are 0.1, 0.3, 0.6, and 1.0 m, respectively.

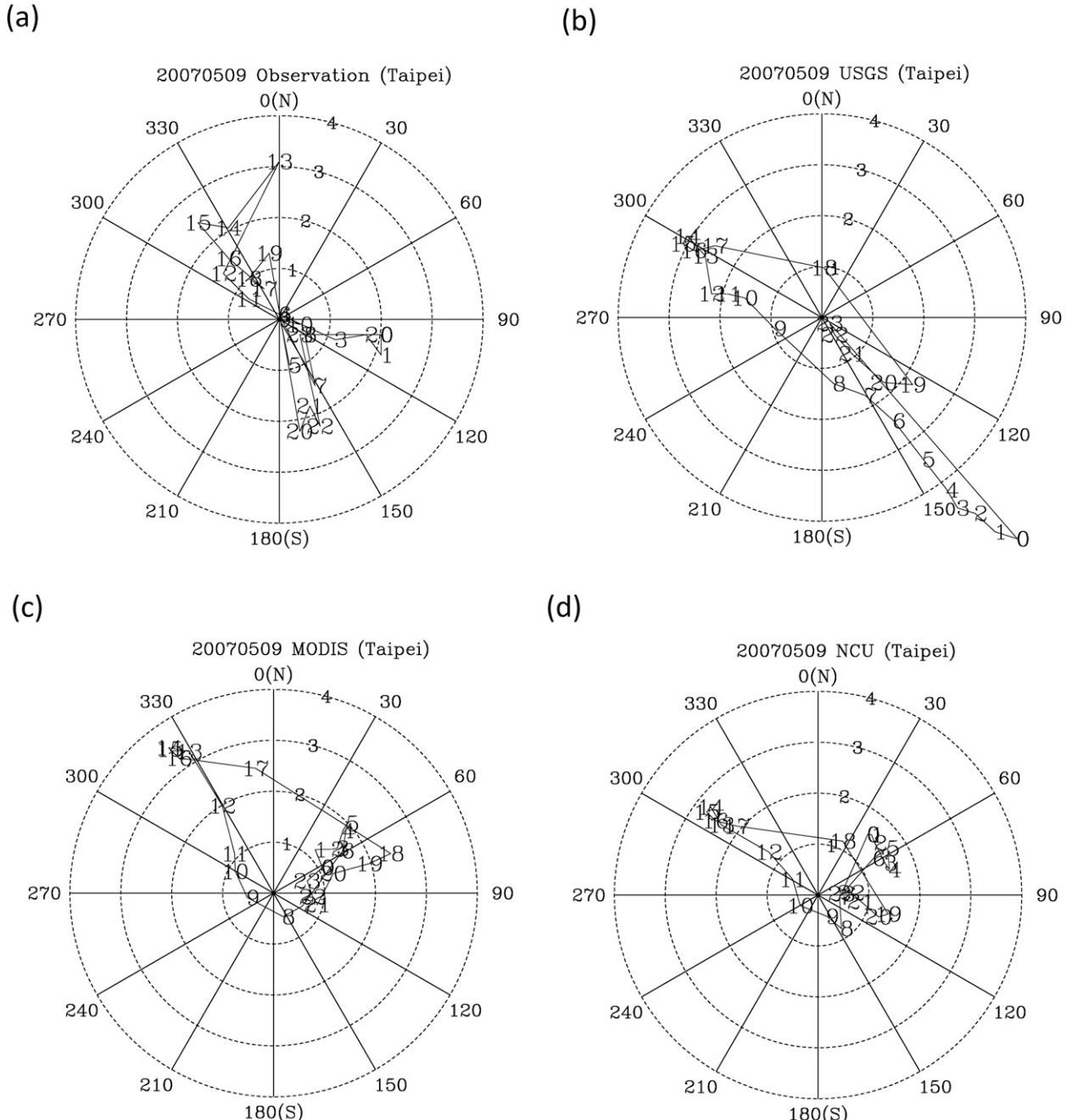


FIG. 16. Hodograph comparison at the Taipei site for 9 May 2007 from (a) observations, (b) WRF-USGS, (c) WRF-MODIS, and (d) WRF-NCU. The arrows pointing from the center to the number identifier (0–23) represent the wind direction at the listed hour. The distance from the center to the number identifier indicates the wind speed ( $\text{m s}^{-1}$ ) as given by the concentric circles.

#### *d. Hodograph analysis*

The hodograph plot was generated to demonstrate the LSB circulation. Figure 16 shows the comparison at the Taipei site on 9 May. The observed data clearly showed a southeasterly flow during the night and morning hours that became stagnant from 0800 to 1000 LST and turned

to northwesterly flow along with the onset of the onshore sea-breeze flow from 1000 to 1100 LST. The simulations all show a clockwise turning of the wind direction on 9 May. Compared to the observed data, the turning of the wind direction occurred 1–2 hours earlier in both the WRF-USGS and WRF-MODIS simulations (around 0800–1000 LST) (Figs. 16b and 16c). The turning

TABLE 3. RMSE comparison of temperature ( $T$ ;  $^{\circ}\text{C}$ ) and wind speed (WS;  $\text{m s}^{-1}$ ) at the Taipei and Chiayi sites.

RMSE	USGS		MODIS		NCU	
	$T$	WS	$T$	WS	$T$	WS
Taipei	1.08	3.03	1.06	1.34	0.99	1.32
Chiayi	1.25	1.29	2.63	0.97	1.14	1.18

of the wind direction was better simulated by WRF-NCU, where it took place between 1000 and 1100 LST, close to the onset time of the sea-breeze flow. The nighttime wind shifted slightly toward the northeasterly direction in the WRF-MODIS and WRF-NCU simulations. The southeasterly offshore flow was better simulated by WRF-USGS; however, the nighttime wind speed was overestimated.

#### e. Statistical analysis

Table 3 shows the root-mean-square error (RMSE) comparison for temperature and wind speed at the Taipei and Chiayi sites. At the Taipei site, the WRF-NCU run exhibited the best performance for both temperature and wind speed. At the Chiayi site, WRF-NCU showed good statistical scores for temperature, while WRF-MODIS produced the worst comparison. Both WRF-MODIS and WRF-NCU exhibited better statistical scores for wind speed than WRF-USGS. The RMSE value of wind speed from the WRF-USGS run was large, particularly at the Taipei site.

Table 4 shows the bias and RMSE comparison of the temperature and wind speed for all the CWB surface sites, the locations of which are illustrated in Fig. 1c. WRF-MODIS (WRF-USGS) overpredicted (underpredicted) temperature, while WRF-NCU agreed best with the observed data. For the wind speed comparison, WRF-USGS showed the least agreement, while the other two runs were comparable. The calculation of the bias and RMSE values for all the surface sites indicated that surface temperature and wind speed prediction could be improved with the updated and accurate NCU LU-LC data.

## 5. Summary and conclusions

The default USGS data currently utilized in WRF modeling systems classify most of the LU types in Taiwan as irrigated croplands and erroneously locates forestlands. An alternative LU dataset retrieved from 2001 MODIS satellite products correctly identified the majority of LU-type distributions, except the extremely urban nature of the western side of the country. Both the USGS and MODIS datasets misrepresented the LU-LC

TABLE 4. Bias and RMSE comparison of temperature ( $^{\circ}\text{C}$ ) and wind speed ( $\text{m s}^{-1}$ ) for all observed surface sites in Taiwan.

	USGS	MODIS	NCU
$T$ (bias)	-0.53	0.357	-0.133
WS (bias)	1.145	0.520	0.628
$T$ (RMSE)	1.924	1.969	1.856
WS (RMSE)	2.215	1.758	1.7946

types in Taiwan, while the new NCU LU data correctly reflected the recent development of urban structures as well as the distributions of croplands and forestlands.

The WRF simulation results with respect to different LU-LC datasets demonstrated that the usage of different LU-LC data modified surface energy fluxes, surface meteorological parameters, and LSB circulation. For a typical day dominated by the local LSB circulation on 9 May 2007, WRF-MODIS predicted the highest temperature in western Taiwan; WRF-USGS predicted the lowest, while the WRF-NCU results fell between the other two simulations. The onshore sea-breeze flow was the strongest in the WRF-MODIS simulation due to the enhanced temperature gradient predicted over western Taiwan. Over land areas, the wind speed was strongest in WRF-USGS but was reduced significantly in WRF-MODIS and WRF-NCU due to the specification of longer roughness length elements that would have increased the surface drag and slowed wind flow. The onset time of the onshore sea-breeze flow was better simulated by the WRF-NCU simulation at the Taipei site.

Comparison with the observed surface datasets indicated overprediction of the temperature by WRF-MODIS, underprediction by WRF-USGS, and best agreement with WRF-NCU. For the wind speed comparison, WRF-USGS consistently overpredicted throughout the whole episode, while WRF-MODIS and WRF-NCU were in better agreement with the observed data. The statistical analysis demonstrated that WRF-NCU outperforms the other simulations. In addition, a flux measurement site located at the Chiayi site allowed us to evaluate the simulated surface flux components. All three runs overpredicted SHF, with the highest bias from WRF-MODIS. Both WRF-USGS and WRF-NCU showed good agreement between the simulated LHF and the observed value.

The NCU LU-LC data lie between two extreme and apparently incorrect LU-LC data points from the USGS and MODIS classifications. The more accurate representation of the NCU LU-LC databases in the area of Taiwan successfully improved local-scale meteorological simulations, particularly for the wind speed and temperature fields. The results indicate the need for

accurate LU data to adequately simulate the surface energy budget, surface meteorological fields, and LSB dynamics in Taiwan. The application of the correct LU–LC datasets is expected to improve numerical weather simulations and enhance weather forecasting capability in the Taiwan area.

**Acknowledgments.** This study was supported by the research project “Study effect of land surface processes on boundary layer meteorological simulation in Taiwan” supported by the National Science Council, Taiwan, under Grant NSC-98-2111-M-008-024-MY2.

## REFERENCES

- Chen, F., and J. Dudhia, 2001: Coupling an advanced land surface–hydrology model with the Penn State–NCAR MM5 modeling system. Part I: Model implementation and sensitivity. *Mon. Wea. Rev.*, **129**, 569–585.
- Cheng, F.-Y., and D. W. Byun, 2008: Application of high resolution land use and land cover data for atmospheric modeling in the Houston–Galveston metropolitan area: Part I, Meteorological simulation results. *Atmos. Environ.*, **42**, 7795–7811.
- , S.-C. Chin, and T.-H. Liu, 2012: The role of boundary layer schemes in meteorological and air quality simulations of the Taiwan area. *Atmos. Environ.*, **54**, 714–727.
- Civerolo, K., and Coauthors, 2007: Estimating the effects of increased urbanization on surface meteorology and ozone concentrations in the New York City metropolitan region. *Atmos. Environ.*, **41**, 1803–1818.
- Dudhia, J., 1989: Numerical study of convection observed during the Winter Monsoon Experiment using a mesoscale two-dimensional model. *J. Atmos. Sci.*, **46**, 3077–3107.
- Grossman-Clarke, S., J. A. Zehnder, W. L. Stefanov, Y. Liu, and M. A. Zoldak, 2005: Urban modifications in a mesoscale meteorological model and the effects on near-surface variables in an arid metropolitan region. *J. Appl. Meteor.*, **44**, 1281–1297.
- Hong, S.-Y., Y. Noh, and J. Dudhia, 2006: A new vertical diffusion package with explicit treatment of entrainment processes. *Mon. Wea. Rev.*, **134**, 2318–2341.
- Kain, J. S., and J. M. Fritsch, 1993: Convective parameterization for mesoscale models: The Kain–Fritsch scheme. *The Representation of Cumulus Convection in Numerical Models*, Meteor. Monogr., No. 46, Amer. Meteor. Soc., 165–170.
- Klemp, J. B., W. C. Skamarock, and J. Dudhia, 2007: Conservative split-explicit time integration methods for the compressible nonhydrostatic equations. *Mon. Wea. Rev.*, **135**, 2897–2913.
- Lam, J. S. L., A. K. H. Lau, and J. C. H. Fung, 2006: Application of refined land-use categories for high resolution mesoscale atmospheric modeling. *Bound.-Layer Meteor.*, **119**, 263–288.
- Lin, C. Y., W. C. Chen, P.-L. Chang, and Y. F. Sheng, 2011: Impact of the urban heat island on precipitation over a complex geographic environment in northern Taiwan. *J. Appl. Meteor. Climatol.*, **50**, 339–353.
- Liu, K.-Y., Z. Wang, and L. F. Hsiao, 2002: A modeling of the sea breeze and its impacts on ozone distribution in northern Taiwan. *Environ. Model. Software*, **17**, 21–27.
- Lo, C. P., and D. A. Quattrochi, 2003: Land use and land cover change, urban heat island phenomenon, and health implications: A remote sensing approach. *Photogramm. Eng. Remote Sens.*, **69**, 1053–1063.
- Michalakes, J., S. Chen, J. Dudhia, L. Hart, J. Klemp, J. Middlecoff, and W. Skamarock, 2001: Development of a next generation regional weather research and forecast model. *Developments in Teracomputing: Proc. Ninth Workshop on the Use of High Performance Computing in Meteorology*, Singapore, ECMWF, 269–276.
- Mlawer, E. J., S. J. Taubman, P. D. Brown, M. J. Iacono, and S. A. Clough, 1997: Radiative transfer for inhomogeneous atmospheres: RRTM, a validated correlated- $k$  model for the longwave. *J. Geophys. Res.*, **102**, 16 663–16 682.
- Noilhan, J., and S. Planton, 1989: A simple parameterization of land surface processes for meteorological models. *Mon. Wea. Rev.*, **117**, 536–549.
- Stull, R. B., 1988: *An Introduction to Boundary Layer Meteorology*. Kluwer Academic, 670 pp.
- Tai, L.-H., J.-S. Hong, B.-J. Tsuang, J.-L. Tsai, and P.-J. Ni, 2008: Update of Taiwan land-use data in WRF model. *J. Atmos. Sci.*, **36**, 43–61.
- Tsai, J.-L., B.-J. Tsuang, and P.-S. Lu, 2007: Surface energy components and land characteristics of a rice paddy. *J. Appl. Meteor. Climatol.*, **46**, 1879–1900.